Jurnal Polimesin
Department of Mechanical Engineering
State Polytechnic of Lhokseumawe
http://e-jurnal.pnl.ac.id/polimesin
e-ISSN : 2549-1999 No. : 2 Month : April
p-ISSN : 1693-5462 Volume : 23 Year : 2025

Processing dates: received on 2025-01-09, reviewed on 2025-04-11, accepted on 2025-04-23 and online availability on 2025-04-30

Analysis of mechanical properties, microstructure, and distortion of Al6061-T6 alloy plate using GTA and GMA welding process

Suherman[1,*], Muharnif M[1], Yusuf Lubis[1], M.A.S Pohan[1], Rakha R Aulia[1], Rizki M. Ali[1], Ilmi[2], Marzuki[3], W.H. Azmi[4]

[1]Departement of Mechanical Engineering, University of Muhammadiyah Sumatera Utara, Medan 20238, Indonesia

[2]Departement of Mechanical Engineering, University of Sumatera Utara, Medan 20155, Indonesia

[3]Engineering Technology of Welding and Fabrication, Lhokseumawe State Polytechnic, Lhokseumawe 24301, Indonesia

[4]Faculty of Mechanical & Automotive Engineering Technology, University of Malaysia Pahang Al-Sultan Abdullah, 26600 Pekan, Pahang, Malaysia

*Corresponding Author: suherman@umsu.ac.id

Abstract

This study compares the effect of filler metal and welding current of Gas Tungsten Arc Welding (GTAW) and Gas Metal Arc Welding (GMAW) on Aluminum alloy Al6061-T6. Three different filler metals, ER4043, ER4047, and ER5356, were used with the GTAW welding process. The welded joints were created at three different welding currents (120, 130, and 140 A) by the GMAW with filler metals ER5356. Optical and Scanning Electron Microscopy (SEM) is used to analyze the surface fracture of impact test welding joints. The results showed that the GMAW process had the most optimum Ultimate Tensile Strength (UTS) compared to the GTAW welding joint, especially for welding current 130 A. The impact strength of ER4047 filler metal with the GTAW process is higher than other joints (61 J/cm2). Optimum conditions were obtained by the GMAW welding process using a welding current of 130 A with maximum tensile strength and impact strength of 350 MPa and 53 J/cm2, respectively. SEM analysis showed that Mg2Si obtained a globular morphology in ER4047 and ER5356 filler metals, and the dimple fracture is indicated at all joints with the GMAW and GTAW processes. Furthermore, increasing welding current by the GMAW process causes higher angular distortion and reduced vickers hardness but does not significantly affect the weld bead. Overall, the GMAW produces better physical and mechanical properties of weld joints than GTAW for all filler metals but results in greater angular distortion.

Keywords:
Al6061, GTAW, GMAW, ER4047, ER5356

1 Introduction

Recently, Aluminum A6061 alloys have been widely used for vehicle structures and automotive [1] [2], naval structures, energy generation, chemical and petrochemical industry [3], shipbuilding (civil and military) [4], automobiles [5, 6], railway transportation [7, 8], aerospace industries [9] and other applications. These alloys are the primary choice due to their good mechanical and forming characteristics [1], weldability, and excellent corrosion resistance [1, 10]. Nowadays, Gas Tungsten Arc Welding (GTAW) and Gas Metal Arc Welding (GMAW) are the most used methods of joining aluminum and its alloys. Generally, the GTAW welding method achieves high-quality joints with minimal spatter [11] and a better weld bead appearance. Several authors have investigated the GTAW process, and different aspects of the process are being studied, including the solidification cracking susceptibility [12], microstructure, and mechanical properties. The most commonly used aluminum alloy joining technique is GMAW. The mechanical properties and microstructure of lap joint welding on aluminum Al6061 using FSW, GTAW, and GMAW methods have been studied by Rathinasuriyan, et al. [13]. They reported that the efficiency and heat input of the FSW method are lower compared to other methods. The FSW method produces smaller grain sizes, resulting in higher tensile strength, hardness, and shear strength than GTAW and GMAW, by 11%, 31%, and 29.75%, respectively.

The GMAW process is a high-efficiency welding process with high heat input and deposition rate [14]. The GMAW process on A6061 T-6 alloy has been widely studied. Soysal et al. [12] studied filler metals on solidification cracking susceptibility. Furthermore, with increases in GMAW current, the hardness of samples increases [15]. The yield strength was reduced by 45.1%, and for Vickers, micro-hardness was 45.2% for 120 amperes. On the other hand, Zhao, et al. [16] found that increases in heat input decrease tensile strength and micro-hardness. The effect of heat input was also studied by [17] on the microstructure and fatigue behavior of Al6061-T6 with the TIG welding process. They are found to increase heat input, grain size, and width of the Heat-Affected Zone (HAZ), but increase Ultimate Tensile Test (UTS). The maximum tensile strength and corrosion rate were achieved at an optimum current of 110 A in GMAW welding of Al6061 alloy [18].

In addition to heat input, filler metals also influence the microstructure, mechanical properties, and fatigue life of Al6061. Arunakumara, et al. [19] also observed the crack propagation rate in Al6061 welds using ER5356 filler metal with the GMAW method. Compared to the HAZ and Base Metal (BM), the weakest fatigue crack growth resistance is in the welding zone. Besides, applying different types of filler metals (ER4043 and ER4553) and T4 heat treatment on GMAW welding of Aluminum Al6061 affects the joint quality. The ER4043 filler metal provides better weld strength than ER4553 [20]. The Post Weld Heat Treatment process increases hardness by 25.6%, tensile strength by 3.8%, and elongation by 21.5% in Al6061 welded using the GMAW method (ER4043) [21]. On the other hand, Soysal and Kou [12] compared filler metals (ER4043 and ER4943) for the solidification cracking of Al6061. The results showed that ER4943 was more effective in reducing solidification cracking than ER4043. Zhou, et al. [22] studied the effect of using ER6183 filler metal on corrosion fatigue of Al6061-T651. Moreover, the flat wire electrode GMAW process improved average micro-hardness by 7.2% and higher tensile properties by 5.96% [23]. Jie, et al. [8] observed welds' fracture morphology and microhardness using the GMAW method with ER5356 filler metals on Al6061 aluminum. In the weld joint, slight precipitation was observed in the weld zone, along with numerous dislocations.

The softening mechanism in the HAZ caused by the welding thermal cycle triggers precipitation hardening vulnerability, leading to a decline in mechanical properties [24]. According to Ramaswamy, et al. [24]The tensile test of Al6061-T6 fractures 12 mm from the weld zone. Vargas, et al. [25] conducted a simulation using FEM to determine failure due to tensile loading on Al6061 weld joints using the GMAW method (filler metal Er 4043). From the experiment, failure was observed in the zone 6-8 mm from the weld center. Furthermore, the corrosion fatigue behavior of aluminum Al6061 weld joints with filler metal Er5183 has been observed by Mutombo and Du Toit [26]. The research results indicate that the GMAW welding process reduces fatigue life, triggering interfacial failure between the HAZ and the Weld Metal (WM) due to larger voids. Han, et al. [27] compared various weld geometries on the fatigue performance of GMAW joints on Al6061. They concluded that full penetration achieved the best fatigue performance in joints.

Recently, aspects of welding parameters include the residual stress and distortion in Al6061-T6 aluminum alloys [28]. The control of distortion and residual stress in thin Al6061 aluminum plates using the GTAW method was proposed by Zhou, et al. [29] with a high-speed hybrid gas flow field. They reported an angular distortion 83.76% lower than conventional welding. Dahiya, et al. [30] investigated the effect of Torch angle, voltage, and wire feed rate on the distortions prediction of Al6063 plates using GMA welding. Jie, et al. [8] evaluated the welding parameter (PWHT) on the microstructure and mechanical properties of welded joints of Al6061-T6 alloy. Whereby Wang, et al. [31] study the effect of PWHT on the microstructure of HAZ. Results show that PWHT has improved mechanical properties, HAZ microstructural recovery, and WM's homogenous microstructure. Furthermore, Fadaeifard, et al. [32] observed the effects of PWHT on Al6061 aluminum using the GTAW method (Er5356 filler). They concluded that PWHT improves the elastic modulus, produces a homogeneous microstructure in the weld zone, and restores the microstructure in the HAZ. Wang, et al. [31] have found that the grain size and precipitation of the welded joint affected the preheat temperature, while the aging temperature enhanced the welded joints' mechanical properties. Rodríguez-Hernández, et al. [3] stated that the GTAW-GMAW hybrid processes result in a reduction in the porosity of WM and higher mechanical properties. The effect of heat treatment on the corrosion behavior of Al6061 aluminum welds has been observed by Nikseresht, et al. [33]. The Heat treatment demonstrated improved corrosion resistance in the weld metal.

It is essential to compare the GTAW and GMAW welding methods on Al6061-T6 for several reasons, as they significantly affect the microstructure and mechanical properties, which in turn impact the joint quality, production efficiency and cost, and corrosion resistance. Previous research has reported comparing welding methods (GTAW and GMAW) on the microstructure and mechanical properties of Al6061 weld joints. However, there is a research gap regarding the effect of different filler metals on the quality of butt joints Al6061 plates, which previous researchers have not explored. In this study, work has been related to comparing the GTAW and GMAW welding processes of AA 6061-T6 plates using (ER4043, ER4047, and ER5356) filler metals. This article focuses on the effect of filler metal and current on mechanical properties such as yield strength, impact strength, Bend test, distortion angle, microstructure analysis, and micro-hardness, and its relationship with GMAW and GTAW process parameters to the width WM and fracture zone from the center line of weld metals.

2 Research methods/ materials and methods

2.1 Material and welding process

In the present investigation, Plate Al6061-T6 aluminum alloys with dimensions (30x 25 x 4 mm) were cut, and further grinding was prepared in a single V grove, as shown in Fig. 1.

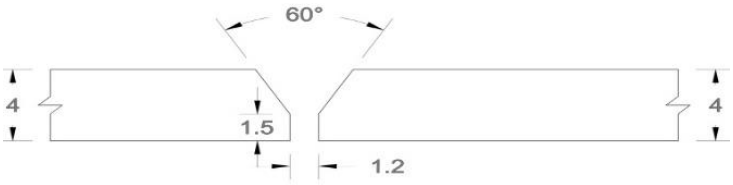

Fig. 1. Single V groove preparation

The Chemical composition of the base material, Al 6061-T6, and filler metals are listed in Table 1. Before the joint of the coupon, the surfaces of the coupon were polished with abrasive paper to remove the oxide film. In this study, aluminum plate welding was carried out using GTAW (Type 250 AC/DC) and GMAW (AUTOMIG Type 273) welding machines (Migatronic™ A/S 9690, Denmark). The welding parameters for the GTAW and GMAW processes are given in Table 2.

Table 1. Chemical composition of Al6061 T6 alloy, ER4043, ER4047, and ER5356 (wt%)

Materials	Si	Fe	Cu	Mn	Mg	Cr	Zn	Ti	Al
Al6061	0.48	0.27	0.18	0.05	0.92	0.09	0.03	0.06	bal
ER4043	4.12	0.43	0.2	0.002	0.006	0.008	0.011	0.018	bal
ER4047	11.2	0.08	0.3	0.15	1.1	-	0.2	-	bal
ER5356	0.12	0.287	0.03	0.05	4.83	0.07	0.008	0.08	bal

Table 2. Welding parameters used in this study

Welding process	Voltage, V	Current, A	Welding speed, mm-s1	Gas flow rate, L min-1	Filler metals	Diameter filler metals (mm)
GMAW 1	17	120	5.76	15	ER 5356	1
GMAW 2	17	130	5.17	15	ER 5356	1
GMAW 3	17	140	5.08	15	ER 5356	1
GTAW 1	12.5	140	5.17	15	ER 4043	2.6
GTAW 2	12.5	140	5.26	15	ER 4047	2.6
GTAW 3	12.5	140	5.08	15	ER 5356	2.6

The test coupon was fixed with the clamp during welding to reduce distortion. Subsequently, coupon tests were joined face to face with a gap of 1-2 mm (Fig. 1). Argon was used as a protective gas in the weld pool for both welding processes.

2.2 Mechanical properties characterization

After the welding test, coupon cut transversal used a band saw apparatus to prepare tensile test specimens, bending test, hardness, impact test, and microstructure, according to Fig. 2. The two samples' tensile and bending tests were measured by Universal Testing Machine MC Model WEW 300D with a loading of 0.02 mm/s.

The impact test (JTM-RP1820-8629) according to ASTM E23 standard sub-size specimens is shown in Fig. 2. A Vickers micro-hardness test was performed with a 100 g load for 15 s using a Future Tech-FM 800 series digital micro hardness tester, cross-section along inline weld metals shown in Fig. 3. The Charpy Impact test method uses 35 kg.f for the GTAW and GMAW specimens, two samples.

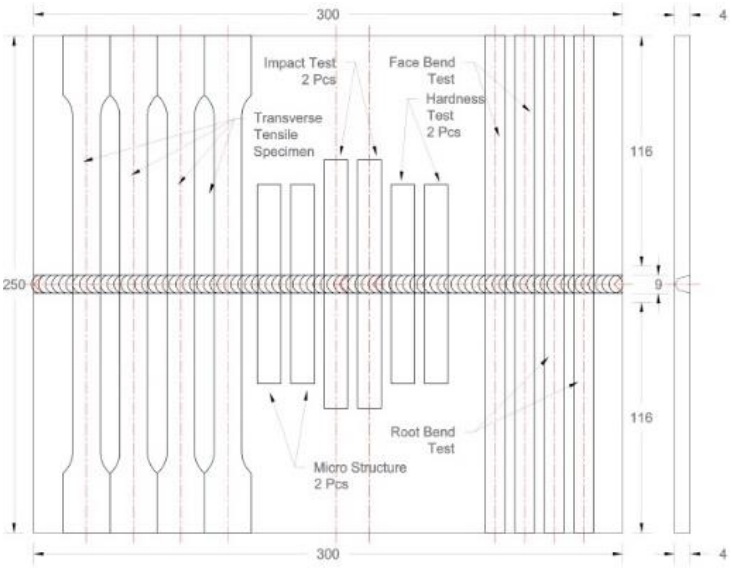

Fig. 2. Schematic of the tensile test, bend test, hardness, impact test, and microstructure

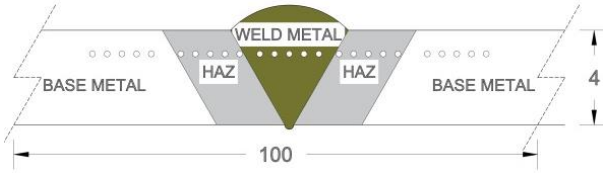

Fig. 3. Micro-hardness test coupon of Al6061-T6

2.3 Width weld, excess weld, and distortion

Measurement distortion of the coupon used Slope Angle Finder (Wipro™) complies with EN 10042 standard, and the excess weld of the coupon is carried out using a welding gauge (WGU7M Nîgata Seiki™). The purpose of distortion measurement on welded plates is to determine the metal deformation caused by thermal expansion and contraction during the welding process. In the case of aluminum, which has high thermal conductivity and a large coefficient of thermal expansion, distortion can be quite significant, especially when using the GMAW method, which involves high heat input Angular distortion measurements were performed on all coupons by placing a Slope Angle Finder on the distorted part of the plate, with the degree of angular distortion indicated by the needle indicator. The plate angle is measured (particularly at the edge or weld joint) before the welding process to obtain an initial reference value by placing the coupon plate horizontally on a known flat table as the zero reference. Next, the Slope Angle Finder is placed on the surface of the coupon plate. After welding and cooling, the coupon is returned to the same position and remeasured using the Slope Angle Finder. The difference in angle (e.g., a change from 0° to 2°) is recorded as an indication of distortion caused by the welding process. The greater the measured angle difference, the higher the level of distortion that has occurred. The width of the weld is measured using a vernier caliper (MITUTOYO™ 530-312).

2.4 Microstructure analysis

The metallographic preparation sample was grinding and polished by machine (Buehler Automate 300) using paper 200, 500, 800, and 1200 and then etched in Keller etchant with an aqueous solution of 0.5 mL HF +100 mL H2O. The micrograph of Welded Metals (WM), HAZ, and the BM used microscope optic metallurgy by Raxvision Material Plus MM10A. The surface fracture of impact test by welding metal GMAW and GTAW welding process was observed and analyzed by SEM (Hitachi TM 3000) at 15 kV. The stages of the research are presented in the research flow diagram, as illustrated in Fig. 4.

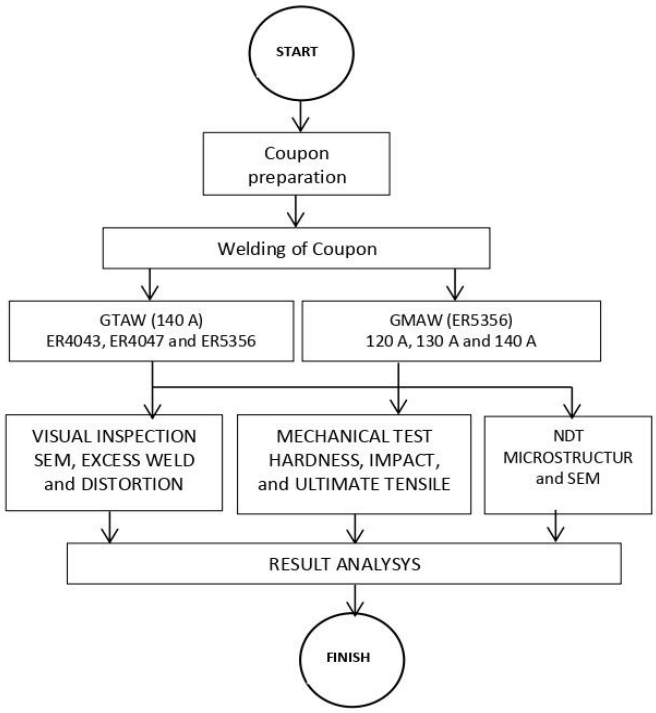

Fig. 4. Research flowchart

3 Results and discussion

3.1 Micro-hardness

Fig. 5 shows the micro-hardness distribution at WM, HAZ, and BM. The hardness of weld metals shown by the GTAW welding process is superior to GMAW. The GTAW generally produces lower heat input compared to GMAW, resulting in a faster cooling rate after welding. This rapid cooling can lead to a finer microstructure and increased hardness in the weld zone. In contrast, GMAW, with its higher heat input, tends to cool more slowly, which can cause grain growth and result in lower hardness in the weld zone [34, 35]. It can be seen that the hardness of the joint GTAW welding process with filler ER4047 and ER5356 is similar.

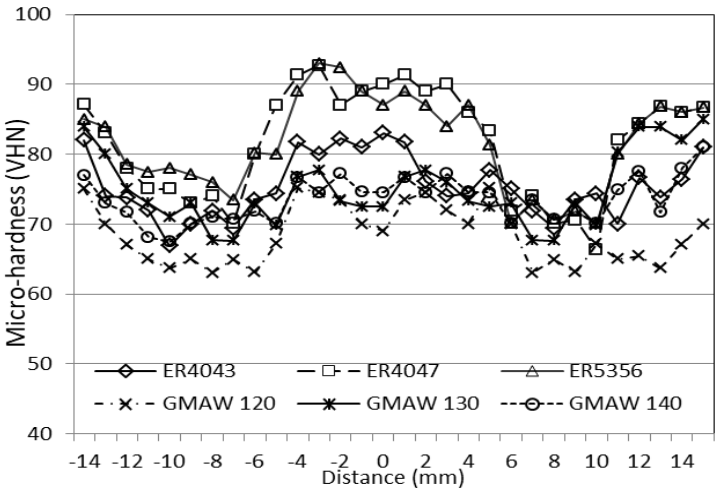

Fig. 5. Micro-hardness distribution GTAW and GMAW process of A6061-T6

With the increased GMAW current, the hardness of the joint decreased. Because of this, the cooling rate and thermal cycle in the weld zone remain quite similar, leading to comparable grain structures and, therefore, similar hardness values. In the range of 120–140 A (for aluminum), the process usually stays within the spray transfer mode (especially with argon shielding). Furthermore, this stable arc condition results in consistent weld bead quality and microstructure, contributing to negligible differences in hardness [36].

The hardness graph shows that the Hardness of The Affected Zone (HAZ) decreased significantly compared to WM and BM, as shown by the micro-hardness profile in Fig. 5. This is due to the increase in grain size in the HAZ and the evaporation of Mg atoms, which leads to the dissolution of the residue and a decrease in hardness [31]. The range between 120 A and 140 A is relatively small, so the overall heat input variation is also limited.

The average distribution hardness is not significantly different from WM (79 HV) and BM (73 HV). The thermal cycle during the weld involves partial dissolution at the heat-affected zone, reducing hardness [4]. A temperature approximation at HAZ 380 ^{o}C produces transformation microstructures, coarsening of β″, and its transformation to β′ phase [24]. The precipitation range depends on the heating and cooling rate.

The hardness value measured in WM indicated that the GTAW process with ER4047 as filler metal (92 Hv) was sample joined at 140 A welding current and 0.167 mm/s welding speed. For example, in the case of WM (ER4047 and ER5356) with the GTAW process (Fig. 4), the average micro-hardness increases slightly (70 HV to 92 HV), which is owing to the solid-solution hardening [37]. This result contradicts the findings of Guzmán, et al. [20], where the hardness value of samples with ER4043 filler metal showed higher hardness than ER5356. This situation may be due to differences in welding parameters such as the welding method, welding current, and heat treatment.

Several factors contribute to the higher hardness values achieved in GTAW welding using filler metals ER4047 and ER5356 compared to ER4043 on Al6061 aluminum alloy. These factors

include filler metal composition, microstructure, and grain size, and differences in precipitate formation. The ER5356 filler metal (Al-Mg) contains approximately 5% magnesium, which contributes to solid solution strengthening and the formation of Mg_2Si precipitates. These precipitates enhance the hardness and strength of the weld joint. On the other hand, ER4047 (Al-Si) contains a high silicon content (12%), which improves molten metal fluidity and resistance to hot cracking, and also contributes significantly to increased hardness [38].

Meanwhile, ER4043 (Al-Si), with approximately 5% silicon, provides good fluidity and hot crack resistance, but its effect on hardness improvement is lower compared to ER4047. The use of ER5356 results in a finer-grain microstructure in the weld zone compared to ER4043 and ER4047. Smaller grain sizes are generally associated with increased hardness and mechanical strength.

3.2 Distortion and excess weld

The welding on components often causes undesirable distortion of Al6061 [39]. Table 3 shows the width of WM, excess weld, and distortion of the coupon of Al6061-T6 with the GTAW and GMAW welding processes. Table 3 shows an increase in welding current by the GMAW welding process, angular distortion, and excess weld metals [28]. The application of restraint in this welding process resulted in a higher angular distortion compared to the findings of Wang et al., amounting to 0.519° [40]. The increased current GMAW generated the distortion of the coupon increased 2° to 7°. The maximum value of angular distortion measured in the Al6061-T6 plate was about 7° with a welding current of 140 amperes, as tabulated in Table 3. The value of angular distortion was similarly studied by Dahiya et al. [30]. Temperature differences between the top and bottom surfaces of the plate cause shrinkage forces across the thickness of the plate near the vicinity of the weld, generating angular distortions during the butt weld of plates [19][28]. Further, Dahiya, et al. [30] stated that angular distortion is also influenced by torch angle, welding speed, wire feed rate, and voltage.

Table 3. Width of weld metal, excess weld, and distortion

Sample	Current (A)	Width of WM (mm)	excess weld (mm)	Distortion (°)
GMAW 120 A	120	9.1	3	3
GMAW 130 A	130	9.1	5	6
GMAW 140 A	140	9.1	5	7
GTAW ER4043	160	9.1	2	2
GTAW ER4047	160	9.1	2	2
GTAW ER5356	160	9.2	2	2

Furthermore, increasing the welding current in the GMAW process increases weld width because of a factor affecting the heat input [41]. Nevertheless, the welding process and increasing welding current in the GMAW process affect the width of weld metal, as shown in Fig. 6.

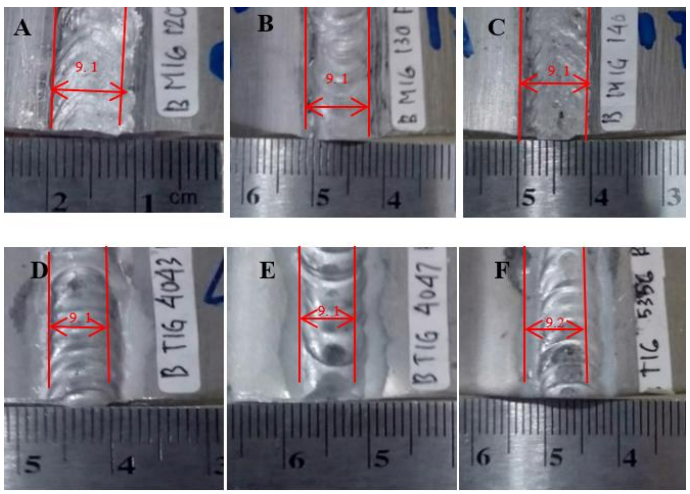

Fig. 6. Weld seams of samples joined by GMAW: (a) GMAW-1, (b) GMAW-2, (c) GMAW-3, (d) GTAW ER4043, (e) GTAW ER 4047, (f) GTAW ER5356

The different filler metals of the GTAW welding process at Al6061-T6 alloy do not require a significant width of weld metal, excess face, and distortion. Furthermore, different GMAW and GTAW welding processes significantly influence weld beads (width and excess weld) in Al6061-T6 alloy. It can be seen that (Table 3) the width joint for both welding's (GTAW and GMAW) is 9 mm, a result similar to the result by [42]. Yürük, et al. [41] reported that the cooling rate and welding speed significantly affect the weld width.

3.3 Ultimate tensile strength test

The Ultimate Tensile Strength (UTS) of Al6061-T6 with GTAW and GMAW welding processes is shown in Table 4. The UTS of BM (476 MPa) is higher than other specimens. On the other hand, heat input could influence the UTS of specimens for GTAW and GMAW welding processes at Al6061-T6; the highest UTS is GMAW with 130 amperes (350 MPa), as shown in Table 4. The differences in welding types and filler metals result in variations in the maximum tensile strength of the test specimens. Tensile test results show that the optimal UTS is achieved using the Er4043 filler metal. These findings align with the research by Guzmán, et al. [20], who compared two different types of filler metals.

Table 4. Failure area of the tensile test of WM

	YS (MPa)	UTS (MPa)	ε (%)	Failure
BM	252	476	3.6	BM
GMAW 120 A	187	344	1.67	HAZ
GMAW 130 A	148	350	3.33	HAZ
GMAW 140 A	183	301	2.6	HAZ
GTAW ER4043	233	326	1.67	HAZ
GTAW ER4047	224	327	1.67	WM
GTAW ER5356	228	320	3.33	HAZ

The increased welding current of the GMAW leads to an increases in grain size [15]. In the GMAW process of A6061-T6, the yield strength and micro-hardness reduction were 36–49%, respectively. The experimental result is similar to the study by Zhao, et al. [16]. According to Table 4, with an increased welding current, the UTS of joints showed a decreasing trend [16]. The lowest UTS was at the specimen with a welding current of 140A. The high heat input causes a coarse dendrite size in the HAZ, growth of precipitates, and microstructure change [37]. Besides, a coarse dendrite size provides a low UTS of the joint due to the Hall-Petch relationship [37]. Samiuddin, et al. [43] [26] found that the increase in heat input produced the formation of Mg_2Si and Al6 (Mn, Fe) intermetallic phases at the grain boundaries, ultimately damaging the weld metal's mechanical properties. All the welded samples obtained were fractured and located in the HAZs, specifically the fracture area, except specimens of the GTAW process with filler ER 4047 (Fig. 7). The HAZ is affected by thermal cycling during welding, so that side is the weakest part and decreases mechanical properties [24].

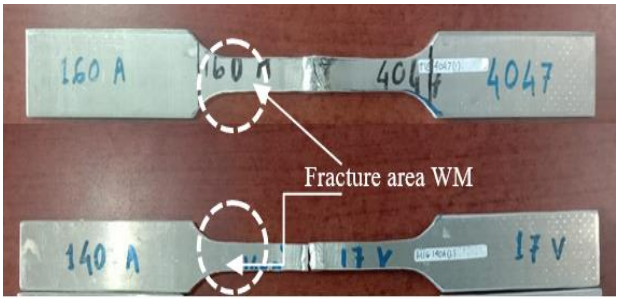

Fig. 7. Fracture area joint Al6061 using GTAW (Er 4047)

Fig. 7 shows the fracture area of the tensile test specimen of GTAW with ER4047 filler metal. The distance of the fracture area at 10-12 mm from the center of the welding bead was observed; the result is similar to that of [42] and farther from the weld center compared to the results of [25], which showed failure at 6-8 mm from the weld center. The increase in the current GMAW welding process widens the failure area (11 to 14 mm) from the center of WM, as

shown in Table 3. The decrease in UTS caused a softened zone in HAZ [24].

During welding, the HAZ experiences thermal cycles that don't melt the metal but do alter its structure. High temperatures in the HAZ can cause grain growth (coarsening), leading to reduced strength and ductility. Further, Al6061 is a precipitation-hardened alloy. The HAZ may reach temperatures high enough to cause dissolution or overaging of strengthening precipitates like Mg_2Si. This reduces hardness and tensile strength specifically in the HAZ region, making it the weakest point in the tensile test. Moreover, the combination of grain coarsening and precipitate dissolution leads to softening in the HAZ [8]. In a tensile test, this softened zone can yield earlier than the surrounding BM or fusion zone, thus reducing the UTS. According to the Hall-Petch relationship, larger grains promote for lower yield strength, which directly affects tensile strength [36].

The UTS of the GTAW welded joint with filler ER4043 was obtained higher than that of ER5356, which contradicts the statement of [44]. The maximum value of elongation measured was obtained with the GTAW process (ER5356) and GMAW processes (130 amperes), as shown in Table 4.

The main factors that contribute to the highest tensile strength achieved by ER5356 (GMAW, 130A) and ER4047 (GTAW) are related to both the welding process and the filler metal properties. GMAW provides a higher deposition rate and deeper penetration than GTAW, especially when using an optimized current of 130A. In addition, ER5356 (containing approximately 5% Mg) offers solid solution strengthening and forms Mg_2Si precipitates, which significantly enhance mechanical properties, including tensile strength. Welding at 130A is likely an optimal condition, providing balanced heat input that results in sound fusion without overheating. It also promotes the formation of fine equiaxed grains and reduces overaging or grain coarsening in the HAZ. In contrast, welding with 120A may lead to incomplete or insufficient fusion, while welding with 140A could produce excessive heat input, causing overaging, coarse-grain growth, and reduced tensile strength.

Welding with ER4047 (GTAW) also results in high tensile strength due to the high silicon content, which improves the fluidity of the molten metal, allowing better spreading and producing defect-free welds. The GTAW process provides better control over heat input and offers a more stable arc, resulting in cleaner welds with minimal defects. Moreover, it produces a narrower HAZ with more controlled microstructural transformation. The combination of refined columnar and equiaxed dendritic structures, along with a more homogeneous microstructure, contributes to enhanced mechanical strength. In comparison, ER4043 (GTAW), which contains lower silicon content, results in a less refined structure and offers less eutectic strengthening. Additionally, ER4043 is more susceptible to solidification cracking in Al6061 due to its lower fluidity compared to ER4047.

3.4 Impact strength

Table 5 shows the impact strength of the GTAW and GMAW welding processes on Al6061-T6 with different filler metals. The impact strength is the highest by the GTAW process with filler metals ER4047 joint and the other weld metals. The maximum impact strength value with the GTAW welding process using ER4047 is higher than 69% compared to raw materials (36 J/cm^2 to 61 J/cm^2).

Moreover, the GMAW process with ER5356 current 130 A increased by 47 % impact strength (36 J/cm^2 to 53 J/cm^2), as shown in Fig. 8. The increase in impact strength of welded joint ER5356 filler metal is due to the filler metal's high magnesium content, as tabulated in Table 1. On the contrary, the specimen by GTAW process with various filler metals provides fracture in WM, as shown in Figs 7(e) and 7(f).

Table 5. Failure area of the impact test of WM

	Impact strength (J/cm^2)	Failure
BM	36	-------
GMAW 120 A	39	Fusion line
GMAW 130 A	53	Fusion line
GMAW 140 A	44	Fusion line
GTAW ER4043	33	WM
GTAW ER4047	61	WM
GTAW ER5356	41	WM

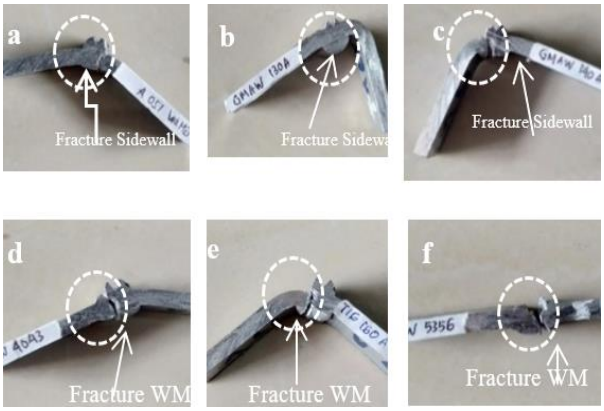

Fig. 8. Fracture of the impact specimen of A6061-T6. (a) GMAW 120 A, (b) GMAW 140 A, (c) GMAW 140 A, (d) GTAW ER4043, (e) GTAW ER4047, and (f) GTAW ER5356

3.5 Microstructural characteristics

Microstructure observations were carried out in WM, HAZ, Partially Melted Zone (PMZ), and BM of Al6061-T6 alloy with three different filler metals, as shown in Fig. 9. It can be seen that the coarse eutectic structure equiaxed grains of α Al (white) and particle β Mg_2Si and Al_2Fe-Si (black) spread uniformly in the BM, as shown in Fig. 9. The GTAW process with ER4043 filler metal provides a microstructure composed of coarse equiaxed dendrite in WM and equiaxed dendrite structure in HAZ, as shown in Figs. 9(b) and 9(c). This result is similar to the finding of Ramaswamy, et al. [24]. The microstructure of WM is an equiaxed grain structure [24].

Moreover, the microstructure of WM with ER4047 filler metal is a typical columnar dendrite structure of coarse sizes, as shown in Figs. 9(d) and 9(e) [37]. The result follows from research by [37]. According to Rajeshkumar et al.[1]Columnar dendrites grow from a Partial Melting Zone (PMZ). Due to different temperature gradients, columnar dendrites grow perpendicular to the fusion lines towards WM [31]. The ER4047 filler metal, which typically consists of aluminum and approximately 11–12% Silicon (Si), plays an important role in the growth of columnar dendrites during welding. Silicon concentrated in the liquid phase tends to promote the formation of columnar dendrites in the central region of the weld pool, leading to an orderly crystal segregation [45]. At certain temperatures, particularly as the molten metal begins to cool and solidify, alloying elements in ER4047, such as silicon, can form dendritic structures. In this case, columnar dendrites are a type of crystal formed during metal solidification. During the solidification process, there are silicon-rich regions that are not easily soluble in the solid phase, resulting in a microstructure with clearly defined columnar dendrites [38]. When these dendritic structures form, the inner region typically consists of a silicon-rich liquid phase, while the outer region consists of a solid phase. In addition, the interaction between the ER4047 filler metal and the base material (Al6061) also influences the element distribution and columnar dendrite growth. During welding, the formation of solid solutions or intermetallic phases may occur, depending on the alloy ratio, which can modify the dendrite shape and element distribution along the weld joint [46].

The high Si content in ER4047 filler metal lowers the eutectic melting point, extends the solidification time, and creates a sharp temperature gradient between the molten and solid metal. This promotes the formation of columnar dendrite growth that follows the thermal gradient direction from the fusion line toward the center of the weld pool.

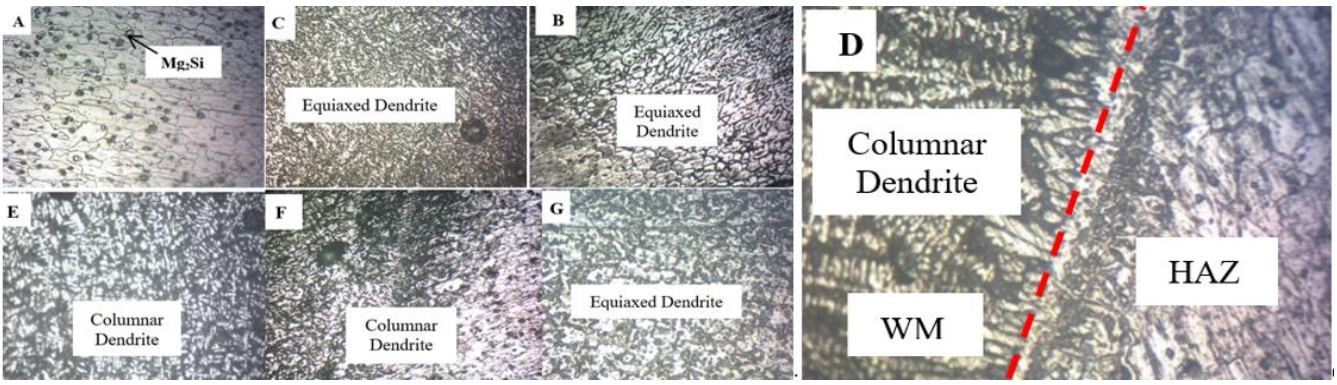

Fig. 9. Microstructures WM, HAZ, and BM (a) BM of Al6061T-6, (b) ER4043, (c) WM ER4043, (d) ER4047, (e) WM 4047, (f) ER5356, and (g) WM 5356

Furthermore, ER4043 contains a lower amount of silicon, resulting in a less pronounced temperature gradient compared to ER4047. In the case of ER5356, which contains magnesium, no eutectic reaction like silicon occurs, leading to a faster and more isotropic solidification process. This results in an equiaxed structure, where crystals grow randomly in various directions, typically due to rapid cooling and uniform nucleation.

In addition, the formation of columnar dendrites is also influenced by the temperature gradient (G) and solidification rate (R). A columnar structure tends to form when there is a high temperature gradient and a slow growth rate at the solid-liquid interface. A combination of high G and low R promotes unidirectional crystal growth (columnar dendrites). In ER4047, this is highly likely, as the silicon-rich liquid remains molten for a longer time, allowing for continued columnar dendrite growth.

Furthermore, the microstructure of WM with ER5356 filler metal is typical equiaxed grains, as shown in Figs. 9(f) and 9(g). This result follows what was reported by Rajeshkumar et al. [1]. The microstructures of HAZ dendritic-like structures are dendrite equiaxed [22]. Most of the microstructure of joints is dendritic-like, thus producing a low UTS. Because of the thermal gradient, solidification growth and cooling rate significantly affect WM's dendrite size and morphology [31].

The Al–5%Si content in ER4043 affects the dendritic structure by forming columnar dendrites in the region near the fusion zone due to directional cooling and growth from the fusion boundary toward the center. Furthermore, ER4047 (Al–12%Si) influences the dendritic structure by increasing the number and length of columnar dendrites due to a higher solidification differential and forming more Al–Si eutectic structures at the dendrite boundaries. Fine equiaxed dendrite structures may form in weld regions with rapid cooling in certain areas, depending on the solidification rate. The use of ER5356 (Al–5%Mg) in welding Al6061 affects the dendritic structure by promoting the formation of predominantly equiaxed dendrites due to more isothermal solidification and a lower temperature gradient, resulting in a more homogeneous microstructure if cooling is sufficiently uniform.

Fig. 10 shows a micrograph of BMs, WM, and HAZ with three different welding currents, 120 A, 130 A, and 140 A. Results showed the difference in dendrite size in WM and HAZ of Al6061-T6. The GMAW process of Al6061-T6 with current 120 A obtained a fine dendrite structure (12 µm) compared to other dendrite sizes of 12.59 µm and 14 µm. With the increasing GMAW current welding process, the dendrite size of WM increased by approximately 12 µm to 14 µm. When the current for GMAW increased, heat input also increased, and with a slower cooling rate, thus producing coarse dendrites in WM and HAZ. The coarse dendrite size gives a lower UTS of the joint, evidence that joint 140 A is lower than to others currently (Table 3). Moreover, the coarse grains in WM of the specimen using welding current (140 A) generated a fracture at WM. On the other hand, the dendrite size in HAZ of 120 A is lower than 130 A and 140 A.

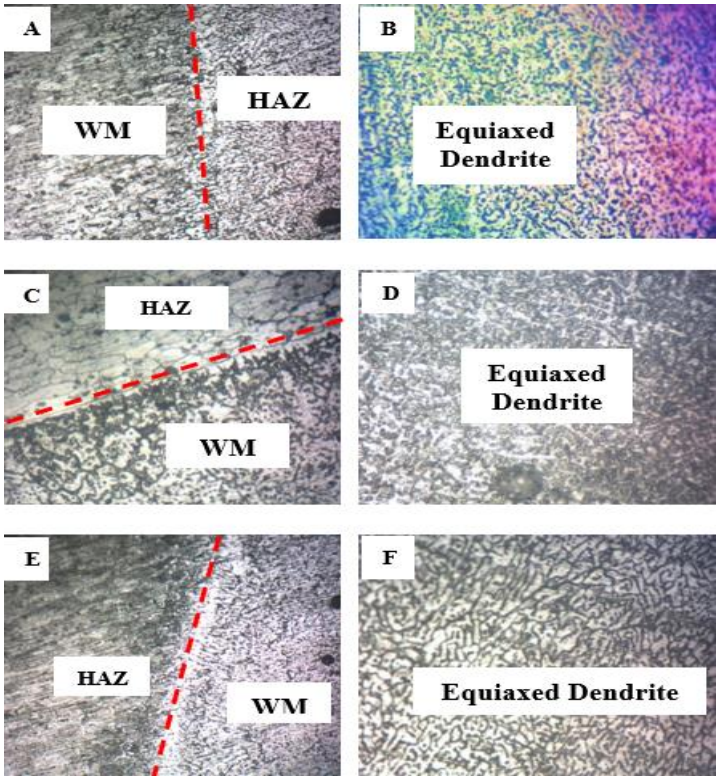

Fig. 10. Optical micrographs a) 120 A, b) WM 120 A, c) 130 A, d) WM 130 A, e) 140 A, f) WM 140 A with GMAW process

3.6 SEM analysis of GTAW and GMAW processes

Fig. 11 shows the SEM images of BM and surface fracture in WM by the GTAW process for Al6061-T6 varied filler metals (ER4043, ER4047, and ER5356).

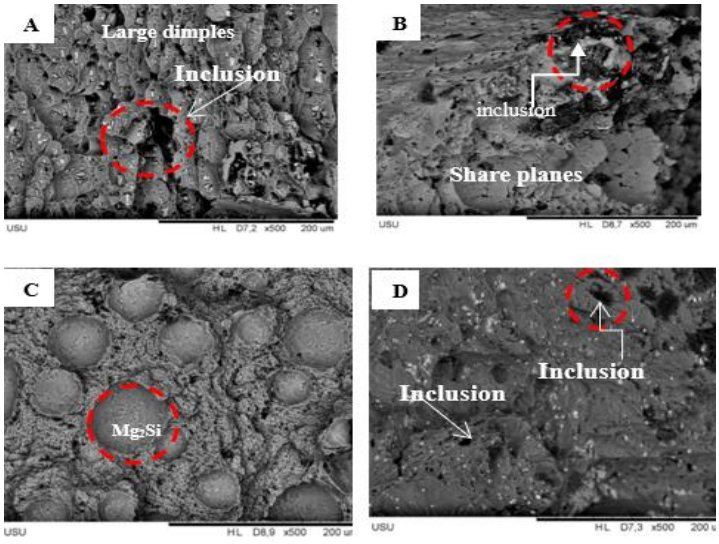

Fig. 11. SEM images of fracture surface impact specimen a) Al6061-T6 (b) GTAW ER4043, (c) GTAW ER5356, (d) GTAW ER4047

It can be seen that the surface fracture of Al6061-T6 dimples fractures (Fig. 11a). In general, the fracture surface forms dimples that are uniformly distributed.

However, the dimples on the ER5356 specimen are smaller than the others. As reported, the dimple's size dramatically affects the weld's toughness and tensile strength [37, 43]. Besides, porosity disperses in weld metals; the pore diameter was 20-30 μm (Fig. 11). The GTAW welding process can lead to micro-porosity defects [16]. The pore-caused hydrogen gas in the form of bubbles is entrapped by solidification during welding [42]. The solubility of molten aluminum increases with increasing welding current, thereby increasing the hydrogen absorbed in the weld pool [17]. Nevertheless, the failure is attributable to the porosity in the WM and acts as a stress concentration and crack initiation [3].

The SEM observed fracture surface morphology after the impact test of weldments (Fig. 11). It is seen due to the micro-cavities and large dimples to evidence a typical morphology of a ductile fracture (Fig. 11a). Large dimples and shallowness were also found on the fracture surface of the GTAW welded joint with ER4047 filler metal (Fig. 11d) [47].

The coarse dimples and quasi-cleavage are uniformly distributed on the fracture surfaces of GMAW welded joints with various welding currents (120A to 140A). The Surface fracture has many dimples of different sizes and depths [44]. The average diameter of the dimples was approximately 10μm shown in Fig. 12 [8]. Interestingly, the morphology of Mg_2Si globular was also found in the specimen by the GMAW process (Fig. 12), but it was large compared to the GTAW welded joint with ER4047 filler metal.

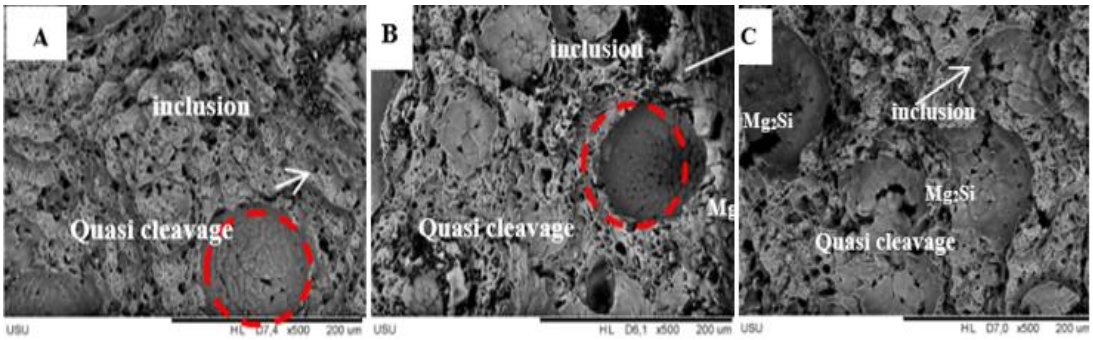

Fig. 12. SEM images of fracture surface impact a) GMAW 120A, b) GMAW 130A, c) GMAW 140A

4 Conclusions

The Tensile strength of the joint reached the maximum value with ER5356 filler metal at welding current 130-ampere GMAW welding process and ER4047 filler wire GTAW process (354 MPa and 332 MPa), respectively. The difference in current strength in GMAW welding does not significantly affect the hardness value of the weld metal. GTAW welding with filler metals ER4047 and ER5356 produced the highest hardness values. The highest impact strength was obtained using filler metal ER4047 GTAW compared to the other specimens. Next, the microstructure of all weld metals shows an equiaxed structure except for the filler metal ER4047, which produces coarse columnar dendrite structures. Besides, welding of welded joints performed using a gas metal arc failed at the interface between the WM and the HAZ when the impact test load. The best impact strength was obtained on the specimen using GTAW with filler metal ER4047.

Furthermore, the tensile test was conducted in the weld joint with two different GTAW and GMAW welding processes, generating the failure area found (11 to 14 mm) from the center WM, except at the welded joint performed using ER4047 by GTAW process and welding current 120 amperes with GMAW welding process. The increasing welding current of the GMAW process enhances angular distortion and root excess weld. This is because GMAW has less control over heat distribution compared to GTAW. Uneven heat distribution can lead to sharp temperature gradients, which in turn increase the likelihood of distortion in the weld joint. In addition, the GMAW process produces a larger volume of WM due to the continuous use of a consumable wire electrode. This larger volume of WM increases the amount of material that undergoes thermal expansion and contraction, thereby raising the potential for distortion [48]. Different filler metals by the GTAW welding process do not significantly distort and width weld bead. Overall, the fracture surface morphology of the impact test showed a dimpled fracture in the WM of all samples, except samples ER4043 and ER5356 with the GTAW process. Finally, the GMAW process using 130 A is most suitable for butt weld Al6061-T6 plate.

Acknowledgements

The author extends gratitude to Universitas Muhammadiyah Sumatera Utara for funding this research under contract number 053/II.3-AU/UMSU-LP2M/C/2022 in 2022.

References

[1] R. Rajeshkumar, V. Niranjani, K. Devakumaran, and K. Banerjee, "Evolution of non-dendritic equiaxed zone and its influence on mechanical properties of tungsten inert gas welded dissimilar A6061-T6 and A6082-T6 joint," Materials Letters, vol. 303, p. 130569, 2021.

[2] Y. Jie, J.-m. Zhang, S.-f. Cao, and P.-c. Guo, "Effect of welding sequence on residual stress and deformation of 6061-T6 aluminium alloy automobile component," Transactions of Nonferrous Metals Society of China, vol. 29, no. 2, pp. 287-295, 2019.

[3] T. Rodríguez-Hernández et al., "First assessment on the microstructure and mechanical properties of gtaw-gmaw hybrid welding of 6061-t6 AA," Journal of Manufacturing Processes, vol. 59, pp. 658-667, 2020.

[4] H. Wang, X. Liu, and L. Liu, "Research on laser-TIG hybrid welding of 6061-T6 aluminum alloys joint and post heat treatment," Metals, vol. 10, no. 1, p. 130, 2020.

[5] L. Zhang, H. Zhong, S. Li, H. Zhao, J. Chen, and L. Qi, "Microstructure, mechanical properties and fatigue crack growth behavior of friction stir welded joint of 6061-T6 aluminum alloy," International Journal of Fatigue, vol. 135, p. 105556, 2020.

[6] M. Kumar, A. Das, and R. Ballav, "Influence of the Zn interlayer on the mechanical strength, corrosion and microstructural behavior of friction stir-welded 6061-T6 aluminium alloy and AZ61 magnesium alloy dissimilar joints," Materials Today Communications, vol. 35, p. 105509, 2023.

[7] D. Priyasudana, S. A. Crisdion, P. Puspitasari, and D. D. Pramono, "Double side friction stir welding effect on mechanical properties and corrosion rate of aluminum alloy AA6061," Heliyon, vol. 9, no. 2, 2023.

[8] Y. Jie, W. Guan, S.-k. Li, Z.-w. Liu, and Y.-l. Gong, "Effect of post-weld heat treatment on microstructure and mechanical properties of welded joints of 6061-T6 aluminum alloy," Transactions of Nonferrous Metals Society of China, vol. 29, no. 10, pp. 2035-2046, 2019.

[9] H. Tu, S. Schmauder, and U. Weber, "Simulation of the fracture behavior of Al6061 laser welded joints with the Rousselier

model," Computational Materials Science, vol. 116, pp. 122-128, 2016.
[10] J. Cheng, Z. Zhang, X. Dong, G. Song, and L. Liu, "A novel post-weld composite treatment process for improving the mechanical properties of AA 6061-T6 aluminum alloy welded joints," Journal of Manufacturing Processes, vol. 82, pp. 15-22, 2022.
[11] R. Rajeshkumar, K. Devakumaran, and K. Banerjee, "Role of interfacial microstructure on mechanical properties of cold metal transfer welded dissimilar A6061-T6 and A6082-T6 joints," Materials Letters, vol. 279, p. 128521, 2020.
[12] T. Soysal and S. Kou, "Effect of filler metals on solidification cracking susceptibility of Al alloys 2024 and 6061," Journal of Materials Processing Technology, vol. 266, pp. 421-428, 2019.
[13] C. Rathinasuriyan, V. S. Kumar, and S. V, "Mechanical and metallurgical properties of GTAW, GMAW and FSW lap joints on AA6061-T6 Alloy," Advances in Materials and Processing Technologies, vol. 8, no. 3, pp. 3231-3247, 2022.
[14] X. Wu, X. Zhao, J. Chen, Z. Zhang, and C. Wu, "Simulation of the influence of welding parameters on weld pool behavior during a TIG-MIG hybrid welding process," Journal of Manufacturing Processes, vol. 79, pp. 460-475, 2022.
[15] C. Chen, G. Sun, W. Du, Y. Li, C. Fan, and H. Zhang, "Influence of heat input on the appearance, microstructure and microhardness of pulsed gas metal arc welded Al alloy weldment," Journal of Materials Research and Technology, vol. 21, pp. 121-130, 2022.
[16] Y. Zhao, F. Chen, S. Cao, C. Chen, and R. Xie, "Effect of CMT welding heat input on microstructure and properties of 2A14 aluminum alloy joint," Metals, vol. 12, no. 12, p. 2100, 2022.
[17] H. Rojas et al., "The impact of heat input on the microstructures, fatigue behaviors, and stress lives of TIG-welded 6061-T6 alloy joints," Materials Research Express, vol. 7, no. 12, p. 126512, 2020.
[18] I. Sabry, A.-H. I. Mourad, and D. T. Thekkuden, "Optimization of metal inert gas-welded aluminium 6061 pipe parameters using analysis of variance and grey relational analysis," SN Applied Sciences, vol. 2, pp. 1-11, 2020.
[19] P. Arunakumara, S. HN, and B. Gautam, "Study of fatigue crack growth of al 6061-T6 welds obtained by gas metal arc welding along longitudinal direction," Cogent Engineering, vol. 11, no. 1, p. 2339469, 2024.
[20] I. Guzmán, E. Granda, J. Acevedo, A. Martínez, Y. Dávila, and R. Velázquez, "Comparative in mechanical behavior of 6061 aluminum alloy welded by pulsed GMAW with different filler metals and heat treatments," Materials, vol. 12, no. 24, p. 4157, 2019.
[21] R. Ahmad and M. Bakar, "Effect of a post-weld heat treatment on the mechanical and microstructure properties of AA6061 joints welded by the gas metal arc welding cold metal transfer method," Materials & Design, vol. 32, no. 10, pp. 5120-5126, 2011.
[22] H. Zhou, F. Fu, Z. Dai, Y. Qiao, J. Chen, and W. Liu, "Effect of laser power on microstructure and micro-galvanic corrosion behavior of a 6061-T6 aluminum alloy welding joints," Metals, vol. 11, no. 1, p. 3, 2020.
[23] K. Sripriyan, M. Ramu, K. Anantharuban, and M. Karthigha, "Characteristic of weld bead using flat wire electrode in GMAW inline during the process: An experimental and numerical analysis," International Journal of Pressure Vessels and Piping, vol. 196, p. 104623, 2022.
[24] A. Ramaswamy, S. Malarvizhi, and V. Balasubramanian, "Influence of Metal Transfer Modes and Postweld Heat Treatment on Tensile Properties of Gas Metal Arc–Welded AA6061-T6 Aluminum Alloy Joints," Materials Performance and Characterization, vol. 9, no. 1, pp. 9-24, 2020.
[25] J. A. Vargas, J. E. Torres, J. A. Pacheco, and R. J. Hernandez, "Analysis of heat input effect on the mechanical properties of Al-6061-T6 alloy weld joints," Materials & Design (1980-2015), vol. 52, pp. 556-564, 2013.
[26] K. Mutombo and M. Du Toit, "Corrosion fatigue behaviour of aluminium alloy 6061-T651 welded using fully automatic gas metal arc welding and ER5183 filler alloy," International Journal of Fatigue, vol. 33, no. 12, pp. 1539-1547, 2011.
[27] S.-W. Han, G. Lee, H. Kim, M.-S. Kim, Y.-R. Jo, and J. Cho, "Effect of weld geometry on fatigue performance of 6061-T6 aluminum GMAW: part 1. Butt joint," Journal of Mechanical Science and Technology, vol. 36, no. 10, pp. 5201-5208, 2022.
[28] A. Khoshroyan and A. R. Darvazi, "Effects of welding parameters and welding sequence on residual stress and distortion in Al6061-T6 aluminum alloy for T-shaped welded joint," Transactions of Nonferrous Metals Society of China, vol. 30, no. 1, pp. 76-89, 2020.
[29] G. Zhou, B. Liu, W. Song, H. Li, J. Kuang, and M. Qiu, "Controlling welding residual stress and distortion of high-strength aluminum alloy thin plates by a trailing hybrid high-speed gas fluid field," Materials, vol. 15, no. 18, p. 6451, 2022.
[30] K. Dahiya, P. Mehrotra, and P. Khanna, "Mathematical modelling to predict angular distortion in MIG welding of aluminium 6063 plates," Materials Today: Proceedings, vol. 62, pp. 3183-3188, 2022.
[31] J. Wang, X. Chen, L. Yang, and G. Zhang, "Effect of preheat & post-weld heat treatment on the microstructure and mechanical properties of 6061-T6 aluminum alloy welded sheets," Materials Science and Engineering: A, vol. 841, p. 143081, 2022.
[32] F. Fadaeifard, K. A. Matori, F. Garavi, M. Al-Falahi, and G. V. Sarrigani, "Effect of post weld heat treatment on microstructure and mechanical properties of gas tungsten arc welded AA6061-T6 alloy," Transactions of Nonferrous Metals Society of China, vol. 26, no. 12, pp. 3102-3114, 2016.
[33] Z. Nikseresht, F. Karimzadeh, M. Golozar, and M. Heidarbeigy, "Effect of heat treatment on microstructure and corrosion behavior of Al6061 alloy weldment," Materials & Design (1980-2015), vol. 31, no. 5, pp. 2643-2648, 2010.
[34] A. Mathivanan, K. Devakumaran, and A. S. Kumar, "Comparative study on mechanical and metallurgical properties of AA6061 aluminum alloy sheet weld by pulsed current and dual pulse gas metal arc welding processes," Materials and Manufacturing Processes, vol. 29, no. 8, pp. 941-947, 2014.
[35] M. Arun and K. Ramachandran, "Effect of welding process on mechanical and metallurgical properties of AA6061 aluminium alloy lap joint," International Journal of Mechanical Engineering and Research, vol. 5, no. 1, 2015.
[36] S. Kou, "Welding Metallurgy Wiley Interscience," Hoboken NJ, 2003.
[37] J. Li, J. Shen, S. Hu, Y. Liang, and Q. Wang, "Microstructure and mechanical properties of 6061/7N01 CMT+ P joints," Journal of Materials Processing Technology, vol. 264, pp. 134-144, 2019.
[38] B. Alzahrani, M. M. Ahmed, M. I. Habba, R. A. Fouad, Y. G. Elshaghoul, and E. A. Gadallah, "TIG Welding of EN AW-6082 Al Alloy: A Comparative Analysis of Filler Rods on Microstructural and Mechanical Performance," Journal of Manufacturing and Materials Processing, vol. 9, no. 1, p. 21, 2025.
[39] H. Hemmatpour and M. Mohtadi-Bonab, "A new approach based on a concurrent cooling method during GTAW and DC-LSND welding to mitigate residual stresses in Al 6061-T6," Journal of Adhesion Science and Technology, pp. 1-19, 2024.
[40] Q. Wang, Y. Zhao, T. Zhao, D. Yan, G. Wang, and A. Wu, "Influence of restraint conditions on residual stress and distortion of 2219-T8 aluminum alloy TIG welded joints based on contour method," Journal of Manufacturing Processes, vol. 68, pp. 796-806, 2021.

[41] A. Yürük, B. Çevik, and N. Kahraman, "Analysis of mechanical and microstructural properties of gas metal arc welded dissimilar aluminum alloys (AA5754/AA6013)," Materials Chemistry and Physics, vol. 273, p. 125117, 2021.
[42] Y. Wang, M. Chen, and C. Wu, "HF pulse effect on microstructure and properties of AC TIG butt-welded joint of 6061Al alloy," Journal of Manufacturing Processes, vol. 56, pp. 878-886, 2020.
[43] M. Samiuddin, J.-l. Li, M. Taimoor, M. N. Siddiqui, S. U. Siddiqui, and J.-t. Xiong, "Investigation on the process parameters of TIG-welded aluminum alloy through mechanical and microstructural characterization," Defence Technology, vol. 17, no. 4, pp. 1234-1248, 2021.
[44] H. Mehdi and R. Mishra, "Investigation of mechanical properties and heat transfer of welded joint of AA6061 and AA7075 using TIG+ FSP welding approach," Journal of Advanced Joining Processes, vol. 1, p. 100003, 2020.
[45] B. Xu, G. Jin, Z. Zhang, J. Wang, and X. Zhan, "Effect on the property of 2195 Al-Li alloy laser-welded joints with different filler materials," Metals, vol. 13, no. 5, p. 958, 2023.
[46] J. Li et al., "Effect of filling materials on microstructure and properties of CMT-laser beam oscillation hybrid welding behavior of dissimilar Al–Mg–Si alloys," Journal of Materials Research and Technology, vol. 26, pp. 8272-8288, 2023.
[47] J. Wang, X. Chen, L. Yang, and G. Zhang, "Sequentially combined thermo-mechanical and mechanical simulation of double-pulse MIG welding of 6061-T6 aluminum alloy sheets," Journal of Manufacturing Processes, vol. 77, pp. 616-631, 2022.
[48] S. Khrais, H. Al Hmoud, A. Abdel Al, and T. Darabseh, "Impact of gas metal arc welding parameters on bead geometry and material distortion of AISI 316L," Journal of Manufacturing and Materials Processing, vol. 7, no. 4, p. 123, 2023.